ASPECTOS ESPECIAIS DA CONSTRUÇÃO DE UM MODELO GEOLÓGICO TRIDIMENSIONAL EM CASO DE VARIABILIDADE LITOFACIAL FORTE DE PLACAS PRODUTIVAS

FEATURES OF CONSTRUCTING A THREE-DIMENSIONAL GEOLOGICAL MODEL IN THE CASE OF STRONG LITHOLOGIC-FACIES VARIABILITY IN DEPOSIT LAYERS

ОСОБЕННОСТИ ПОСТРОЕНИЯ ТРЕХМЕРНОЙ ГЕОЛОГИЧЕСКОЙ МОДЕЛИ В СЛУЧАЕ СИЛЬНОЙ ЛИТОЛОГО-ФАЦИАЛЬНОЙ ИЗМЕНЧИВОСТИ ПРОДУКТИВНЫХ ПЛАСТОВ

KADYROV, Marsel A.[1*]; NEELOVA, Evgeniya Yu.[1]; NIKIFOROV, Artur S.[2]; PONOMAREV, Sergey A.[3]

[1]Tyumen Industrial University, Department of Geology of Oil and Gas Fields, 56 Volodarsky Str., zip code 625000, Tyumen – Russian Federation
(phone: +7 3452 28 36 60)

[2] Tyumen Industrial University, Department of Technospheric Security, 56 Volodarsky Str., zip code 625000, Tyumen – Russian Federation
(phone: +7 3452 28 36 60)

[3] LTD “2gis-Kaliningrad”, 30 Lenin Ave., zip code 236006, Kaliningrad – Russian Federation
(phone: +8 902 251 73 51)

** Corresponding author*
e-mail: Kadyrov-marsel@bk.ru

Received 22 June 2018; received in revised form 26 November 2018; accepted 03 December 2018

RESUMO

O artigo focaliza-se na construção de um modelo geológico tridimensional das camadas produtivas do campo. Um modelo geológico digital tridimensional das camadas produtivas do campo foi construído no pacote de software "IRAP RMS" da versão 2013.1.2. Com base na modelagem geológica, as condições de ocorrência nos estratos produtivos foram especificadas, um quadro estrutural do campo foi construído e, também, foram obtidas distribuições espaciais geologicamente significativas dos parâmetros que descrevem as propriedades litológico-petrofísicas e de filtração e capacitivas do estrato. A veracidade do modelo geológico criado do campo foi avaliada por meio de monitoramento geológico e estatístico em fases dos resultados da distribuição dos parâmetros de modelagem. O modelo geológico pode ser usado para prever indicadores tecnológicos de exploração.

Palavras-chave: *campo, strato, variabilidade litofacial, propriedades de filtração e capacitivas*.

ABSTRACT

The article deals with the construction of a three-dimensional geological model of deposit layers. A digital three-dimensional geological model of productive deposit layers was built in the "IRAP RMS" software package version 2013.1.2. On the basis of geological modeling, the conditions for the occurrence of productive strata have been clarified, the structural framework of the deposit has been constructed, geologically- rich spatial distributions of parameters describing the lithologic-petrophysical and reservoir properties of the reservoir have been obtained. The estimation of the reliability of the created geological model of strata is made by stage-by-stage geological-statistical monitoring of results of distributions in modeling parameters. A geological model can be used to forecast technological development indicators.

Keywords: *deposit, stratum, lithologic-facies variability, filtration-capacitive properties.*

10.52571/PTQ.SI1.2018.315_PeriodicoES.pdf

АННОТАЦИЯ

В статье рассматривается построение трехмерной геологической модели продуктивных пластов месторождения. Цифровая трехмерная геологическая модель продуктивных пластов месторождения строилась в программном комплексе «IRAP RMS» версии 2013.1.2. На основании геологического моделирования, уточнены условия залегания продуктивных пластах, построен структурный каркас месторождения, получены геологически содержательные пространственные распределения параметров, описывающих литолого-петрофизические и фильтрационно-емкостные свойства пласта. Проведена оценка достоверности созданной геологической модели месторождения путем поэтапного геолого-статистического мониторинга результатов распределений параметров моделирования. Геологическая модель может быть использована для прогноза технологических показателей разработки.

Ключевые слова: *месторождение, пласт, литолого-фациальная изменчивость, фильтрационно-емкостные свойства.*

INTRODUCTION

Three-dimensional geological modeling is an integral part of the processing and interpretation of geological and geophysical data. In the process of solving geological problems at different stages of research, it is necessary to construct three-dimensional geological models. In modern packages of geological modeling, as a rule, a large number of construction algorithms are offered for selection (Baimakhan *et al.*, 2009; Kuznetsova *et al.*, 2018; Lomakin *et al.*, 2017). A well-founded choice of methods that takes into account the features of the geological structure of the modeled object (for example, its differential properties or static characteristics), the use of a priori and/or indirect information makes it possible to significantly improve the accuracy of models for a given set of initial data.

The creation of three-dimensional geological models at the present stage is an indispensable element in the design, analysis, and regulation of the development of oil and gas fields (Burgess, 2016; Ogata *et al.*, 2017; Satelles *et al.*, 2018). The task of reliable and high-quality 3D modeling is relevant for the calculation of reserves and the design of technological documents.

All modern modeling software packages contain the following main stages of 3D geological modeling: preparatory stage; structural modeling; creation of a three-dimensional grid; averaging of borehole data into cells of a three-dimensional grid; lithologic-facial modeling; petrophysical modeling; saturation simulation; 3D calculation of reserves.

All stages are interconnected, and the results of each affect both the quality of subsequent steps and the reliability of the entire model as a whole (Gallistl *et al.*, 2018; Gąsiewicz, 2017; McGinnis *et al.*, 2017).

The main reason that facies analysis is practically not used in the practice of 3D modeling is that not every field has data that allows to fully carry out such analysis with bringing it to specific results that could be technologically taken into account in the construction of 3D -Geological model. The second reason is that for the creation of facial models, a large amount of information is needed from different areas of research – regional and local geological information, studied in lithology, sedimentation and FEC core, GIS data, seismic interpretation results, hydrodynamic studies, field development information (Xypolias *et al.*, 2018; Habib *et al.*, 2016). Only an integrated approach, in which all available data are linked to a consistent scheme, will allow the facial analysis to be performed correctly.

MATERIALS AND METHODS

A digital three-dimensional geological model of productive deposit layers was built in the "IRAP RMS" software package version 2013.1.2. In the construction of the geological model, well data (well position information, GIS data, RIGIS data) were used as input data (Zakrevsky, 2009; Zakrevsky, 2012; Belkina *et al.*, 2015; Ababkov *et al.*, 2010; Baranov *et al.*, 2012; Ministry of Energy of the Russian Federation…, 2000; Averbukh *et al.*, 2003; Zakrevsky *et al.*, 2016). Structural models are made by the method of convergence from the reflecting horizon (RH) "IIa" – the bars of the Bazhenov suite, taking into account the zones of

DOI: 10.52571/PTQ.SI1.2018.315_PeriodicoES.pdf

wedging of the seams, revealed at the stage of dynamic analysis of seismic data.

All productive strata were built in a single grid, the layers in the general grid are built in separate sub-strips with an individual approach to cutting along the Z axis, depending on the total thickness of the formation, the minimum size of the permeable interlayer, and the sedimentation characteristics.

The size of the region of structural modeling was chosen based on the expected oil and gas bearing contours and the location of the marginal wells.

The initial information for structural modeling was taken from absolute marks of the stratigraphic roof and the base, the structural map along the top of the RH IIa, identified with the base of the Bazhenov suite.

The size of the cells in constructing the structural surfaces of the model is chosen to be 50 × 50 m.

RESULTS AND DISCUSSION:

2.1. Building a 3D grid

Based on the sedimentation conditions of the modeled sediments, the 3D net of productive strata was constructed by proportional division into strata between the stratigraphic roof and the base. Based on the lateral variability of geological and petrophysical parameters and guidelines for the construction of 3D-geotechnical models mesh sizes given lateral 50 x 50 m (d_x x d_y).

For the strata J_1^1, B_1 and $J_1^{2a,}$ when slicing the mesh along the vertical, additional structural surfaces were used – the corresponding strata were built up from the base with the use of a common thickness of 2 m in the wedging zone. This approach was used to reproduce the erosion surface of terrigenous deposits confined to the strata J_1^1, B_1 and J_1^{2a} (Figure 1)

The vertical size of the cells was calculated based on the minimum thickness of the elementary interlayer, and the sampling step of the GIS record, and was selected so that the well information was transferred to the 3D grid correctly and without distortion. The parameters of the three-dimensional grids are given in Table 1.

2.2. Averaging the borehole data onto a three-dimensional mesh

The next stage in the construction of the model was the transfer of borehole information to the cells of a three-dimensional grid through which the well traverse trajectories.

The wellbore information consists of discrete curves ("ZONELOG" – stratigraphic curve, "LITO_dis" – lithology curve (collector / noncollector), "NOB_dis" – saturation curve) and continuous curves ("Kp" – porosity coefficient parameter curve, "Kn" – the curve of the parameter of the oil saturation coefficient, "Kpr" – the permeability parameter curve, "LITO" – a continuous curve of lithology) . Continuous curves were averaged in accordance with the discrete parameter of lithology, i.e. independently in each code of a discrete curve.

To assess the correctness of the transfer of the original borehole information to the cells of the three-dimensional grid, the histograms and statistical indices of the averaged parameters were compared for each counting object (Figures 2-4). The criterion for the correctness of the operation performed was the prevention of a discrepancy between the initial and averaged parameters (minimum, maximum, average value) of more than 5% relative.

2.3. Construction of a lithological model

Since the initial data on RIGIS materials have a curve characterizing only collector / non-collector values, the model calculates the lithology parameter reflecting these two values: 0 – non-collector, 1 – collector.

As additional information, the sand maps obtained for geological objects (layer $J_1^1 + B_1$ and layer $J_1^{2a+b} + B_2$) through predictive maps of effective thicknesses based on dynamic seismic data analysis using neural networks.

For the purpose of predicting the parameters of the FES for productive layers $J_1^1 + B_1$ and $J_1^2 + B_2$, a dynamic analysis of the seismic record was performed. During time intervals taken in the course of 2015 g of the seismic report. (Figure 5), more than 30 seismic attributes were calculated, none of which gave positive results when constructing dependencies with the values of effective thicknesses at the well points.

Due to low values of the correlation

coefficient between the attributes of the seismic wavefield and the presence of an indirect connection of some attributes with certain classes of values of effective thicknesses based on well data, it was decided to use neural networks to construct predictive maps of effective thicknesses in productive layers.

In neural network modeling, the seismic attributes "*Instantaneous phase", "Half energy", "RMS amplitude" were* used for the productive layer $J_{1-1} + B_1$. The rate of correlation of the effective thickness values from the values of the seismic attribute obtained during the neural network simulation is 0.76 (Figure 6).

In neural network modeling, the seismic attributes "*Instantaneous phase", "Instantaneous frequency", "Sum of amplitudes" were* used for the productive layer $J_{1-2} + B_2$. The rate of correlation of the effective thickness values from the values of the seismic attribute obtained during the neural network simulation is 0.69 (Figure 6). The results of neural network modeling are presented in Figure 7.

The first stage in the construction of the lithological model was the creation of a combined trend cube of sandstone, based on forecast seismic maps of effective thicknesses (Figures 8-9) and statistical indices of the geological and statistical profile of the lithology parameter for well data (RIGIS GSR). This cube was obtained using the "Parameter trend modeling" module of the "IRAP RMS" software package separately for the simulated objects. Later, it was used as the main trend in the distribution of layers identified during the interpretation of GIS data in the inter-well space of the 3D geological model.

The distribution of the continuous parameter of lithology ("NTG") in the inter-well space was carried out in the "Petrophysical modeling" module of the "IRAP RMS" software package through statistical distribution algorithms. Taking into account the densely drilled operational well network, which is associated with a low dependence of the variation of the variogram parameters on the results of the distribution in the cube, the various ranks were chosen empirically and the main criterion was uniform coverage of the distribution within the chosen range of constructions and visual control of the vertical reservoirs in the inter-well space. The cutoff of the discrete cube of lithology is taken equal to 0.5. The resulting effective thickness maps are shown in Figures 10 and 11.

*2.*4. Constructing a cube of the porosity coefficient

The distribution of the porosity coefficient was carried out in the module "Petrophysical modeling". As a trend; we used maps of the distribution of weighted average values of the porosity of 2 D and extremes from well data, individually for each layer. The correctness of the distribution of the porosity coefficient in the three-dimensional space of the geological model (Kp cube) was estimated by comparing the statistical parameters (minimum, maximum, average value) and comparing the resulting distributions of the porosity values on the 3D map cube with maps of the weighted average porosity values of 2D (Figure 12).

2.5. Building a cube of the oil and gas saturation coefficient

2.5.1. Model of the transition zone

To construct the transition zone model, we used the Buckley-Leverett J-function obtained on our own core (Gryshchenko, 2008; Kalmykov *et al.*, 2011; Antipin and Belkin, 2016). The Buckley-Leverett J-function allows us to generalize the values of capillary pressure for samples with different values of porosity and permeability. The Buckley-Leverett J-function has the Equation 1. Where J- Buckley-Leverett's J-function, R_s is the value of the capillary pressure at the interface between the oil and water in atm; K_{pr} is the permeability coefficient, n * 10^{-3} mkm ^{2}; K_p – coefficient of porosity, d. units.; γ – surface tension hydrocarbons / formation water, reference value 27 dyne / cm.

θ is the wettability angle, is equal to 0 because in experiments to determine the capillary characteristics, the extracted samples are used, i.e. hydrophilic, then cos θ = 1.

Since to build capillary curves water from the samples is displaced, as a rule, by air, it is necessary to recalculate the measured capillary pressure to the conditions for the oil-water interface according to Equation 2. Where – $R_s^{(air-water)}$ – the value of capillary pressure at the interface between air and water (laboratory measurements of *Pc* when water is displaced by air), atm; $\theta^{(air-water)}$ and $\theta^{(oil-water)}$ – wetting angles at the relevant interface. The wettability angle is θ = 0 since in experiments to determine the capillary characteristics, the extracted samples

are used, i.e. hydrophilic, then cos θ = 1; $\sigma^{(oil\text{-}water)}$ – surface tension at oil-water interfaces, reference value 27 dynes / cm; $\sigma^{(air\text{-}water)}$ – surface tension at air-water interfaces. The constant, the value is 72 dynes/cm.

Capillary pressure is often defined as "height above free water level" or distance from a pure water mirror (Equation 3). Where δ_v and δ_n – the density of water and oil at reservoir temperature, g / cm ^{3}; 0.098 – gradient of freshwater pressure; h – height above free water level, m; R_s is the value of the capillary pressure, atm.

Thus, conversion of the capillary curve in curve K_v in the height h of the studied interval incision above the level of zero capillary pressure in meters is carried out by the Equation 4. To construct the transition zone, we used data on the capillary pressure curves separately for the reservoir $J_{1\text{-}1} + B_1$ and $J_{1\text{-}2} + B_2$, previously reduced to reservoir conditions.

2.5.2. Layer $J_1^1 + B_1$

According to the core data from the layer $J_1^1 + B_1$, the dependence K_v = f (J-function) was constructed (Figure 13). Thus, the defining Equation 5 for the capillary saturation model has the following form Equation 5. Taking into account the density of oil in the reservoir conditions (0.435 g / cm ^{3}), the equation for calculating Equation 6 takes the following form Equation 6.

2.5.3. Layer $J_1^2 + B_2$

According to the core data from the layer $J_1^2 + B_2$, the dependence K_v = f (J-function) was constructed (Figure 14). As can be seen from the above comparison, collecting solids of layer $J_1^2 + B_2$ has a more complex structure than layer $J_1^1 + B_1$.The application of the algorithm K_{pr} / K_p does not fully allow to generalize all lithotypes of solids .To improve accuracy, we identified three groups of points with a division by the permeability coefficient (Figure 15).

Thus, the defining equations for the capillary saturation model have the following Equations 7,9,10,11. Taking into account the density of oil in the reservoir conditions (0.582 g / cm ^{3}), the equations for calculating take the following Equations 12, 13, 14, 15, 16, 17. Using the trend cube K_{ng}, constructed with the help of these equations, in the module "Petrophysical modeling" of the software complex "IRAP RMS" the distribution of the oil and gas saturation coefficient in the inter-well space of the geological model was performed. To assess the quality of the saturation model, a comparison of the statistical indices (min, max, mean value), histograms of the obtained oil-gas saturation cube with borehole data (Figure 4) and analysis of the resulting maps of the distribution of weighted mean values was carried out for each layer.

CONCLUSIONS:

On the basis of geological modeling, the conditions for the occurrence of productive strata have been clarified, the structural framework of the deposit has been constructed, geologically-rich spatial distributions of parameters describing the lithologic-petrophysical and reservoir properties of the reservoir have been obtained.

The deposit is modeled with a sufficient degree of detail. When creating a geological model, a modern mathematical apparatus of geostatistical and deterministic technologies were used. The estimation of the reliability of the created geological model of strata is made by stage-by-stage geological-statistical monitoring of results of distributions in modeling parameters. At all stages of the construction of the geological model, an analysis was made of the correspondence between the results obtained and the geologic assumptions about the structure of the layers in question. Thus, according to the authors, the geological model can be used to forecast the technological development indicators. Due to the fact that building adequate geological models of oil fields can significantly improve the efficiency of field development, this article outlines the basics of geological modeling based on the use of hydraulic flow units (reservoirs).

The construction of the model is reduced to the following stages: the construction of the lithological-sedimentation model, the allocation of classes of reservoirs and the definition of their relationships with the complex logging data, the calculation of the permeability cube. In contrast to the porosity / permeability distribution models, the constructed model takes into account the contribution of the capacitive heterogeneity of the pore space and allows more accurate calculation of the permeability values in the interwell zones

and in areas not detected by drilling.

REFERENCES:

1. Ababkov, K.V., Suleimanov, D.D., Sultanov, Sh.Kh., Kotenev, Yu.A., Varlamov, D.I. Fundamentals of 3D digital geological modeling, Ufa: Publishing house "Oil and gas business", **2010**.
2. Averbukh, A.G., Bilibin, S.I., Bolotnik, D.N., Velichkina, N.F., Gutman, I.S., Denisov, S.B., Dyakonova, T.F., Zakrevsky, K.E., Serkov, M.H., Starobintsev, A.E., Chernitsky, A.V. *Methodical instructions for the creation of permanent geological and technological models of oil and gas and oil fields. Part 1. Geological models,* Moscow: JSC VNII, **2003**.
3. Baranov, V.E., Kurelenkov, S.Kh., Sheveleva, L.V. *Applied modeling of the reservoir*, Tomsk: TPU, Center for Professional Retraining of Oil and Gas Professionals, **2012**.
4. Belkina, V.A., Bembel', S.R., Zaboeva, A.A., Sankova N.V. *Fundamentals of geological modeling,* Tyumen: Tyumen State Technical University, **2015**.
5. Burgess, P.M. *Geology*, **2016**, *44 (6)*, 443-446
6. Gallistl, J., Weigand, M., Stumvoll, M., Ottowitz, D., Glade, T., Orozco, A.F. *Engineering Geology*, **2018**, *245*, 292-308.
7. Habib, M., Guangqing, Y., Xie, C., Charles, S.P., Jakada, H., Danlami, M.S., Ahmed, H.A., Omeiza, I.A. *Journal of Petroleum Exploration and Production Technology,* **2016**, *7*, 252
8. Kalmykov, G.A., Gimaltdinova, A.F., Topunova, G.G. *Bulletin of Moscow University. Series 4: Geology*, **2011**, *4*, 71-74.
9. Kuznetsova, E.L., Kuznetsova, E.L., Rabinskiy, L.N., Zhavoronok, S.I. *Journal of Vibroengineering*, **2018**, *20(2)*, 1108-1117
10. Lomakin, E.V., Lurie, S.A., Belov, P.A., Rabinskii, L.N. *Doklady Physics*, **2017**, *62(1)*, 46-49
11. McGinnis, R.N., Ferrill, D.A., Morris, A.P., Smart, K.J., Lehrmann, D. *Journal of Structural Geology*, **2017**, *95*, 160-170.
12. Ministry of Energy of the Russian Federation. RD 153-39.0-047-00 Regulation on the creation of constantly operating geological and technological models of oil and gas and oil fields, **2000**. Available at: https://minenergo.gov.ru/node/1575
13. Ogata, K., Storti, F., Balsamo, F., Tinterri, R., Bedogni, E., Fetter, M., Gomes, L., Hatushika, R. Bulletin of the Geological Society of America, **2017**, *129 (1-2)*, 76-92.
14. Satelles, J.L., Bezerra da Silva, H.E., Farias, L.R., Panero, F.D.S. *Periodico Tche Quimica*, **2018**, *15(30)*, 160-176
15. Xypolias, P., Gerogiannis, N., Chatzaras, V., Papapavlou, K., Kruckenberg, S.C., Aravadinou, E., Michels, Z. *Journal of Structural Geology*, **2018**, *115*, 64-81.
16. Zakrevsky, K.E. *Geological 3D modeling*, Moscow: Publishing house of CPI Mask LLC, **2009**.
17. Zakrevsky, K.E. *Workshop on geological 3D-modeling. Building a test model in Petrel 2011*, Moscow: SamGTU, **2012**.
18. Zakrevsky, K.E., Bobrov, A.V., Vorobiev, D.V., Gorkaltsev, A.A., Zalyalieva, A.R., Ivanitsky, M.Yu., Parfenov, N.A., Podnebesnykh, A.V., Popov, V.L., Spindler, A.A., Yakovenko, O.V., Yashkov, D.S. *Geological modeling of the horizon Yu1 of Tomsk region*, Tomsk: TSU Publishing House, **2016**.
19. Baimakhan, R.B., Danaev, N.T., Baimakhan, A.R., Salgaraeva, G.I., Rysbaeva, G.P., Kulmaganbetova, Zh.K., Avdarsolkyzy, S., Makhanova, A.A., Dashdorj, S. *Geotechnical Aspects of Underground Construction in Soft Ground – Proceedings of the 6th International Symposium, IS-SHANGHAI 2008*, **2009**, 751-755.
20. Gąsiewicz, A. *Chemical Geology*, **2017**, *164(3-4)*, 183-218.
21. Antipin, Ya.O., Belkin, V.A. *Territory of OIL & GAS*, **2016**, *2*, 51-57.
22. Gryshchenko, M.A. *Geology of Oil and Gas*, **2008**, *5*, 45-51.

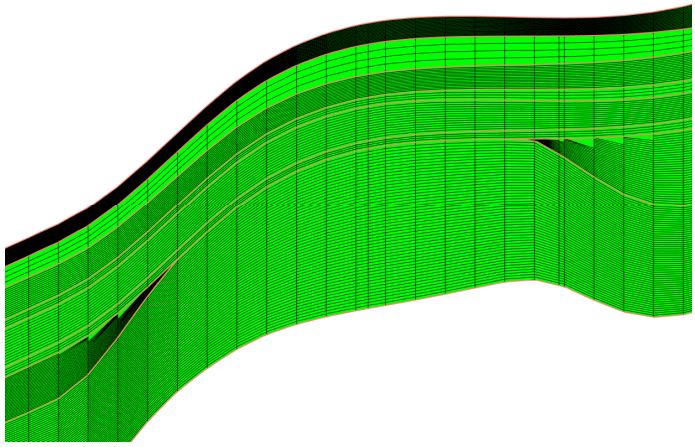

***Figure 1**.Implementation of segmentation of a 3D grid in the area of erosion of deposits of the strata J_1^{2a}*

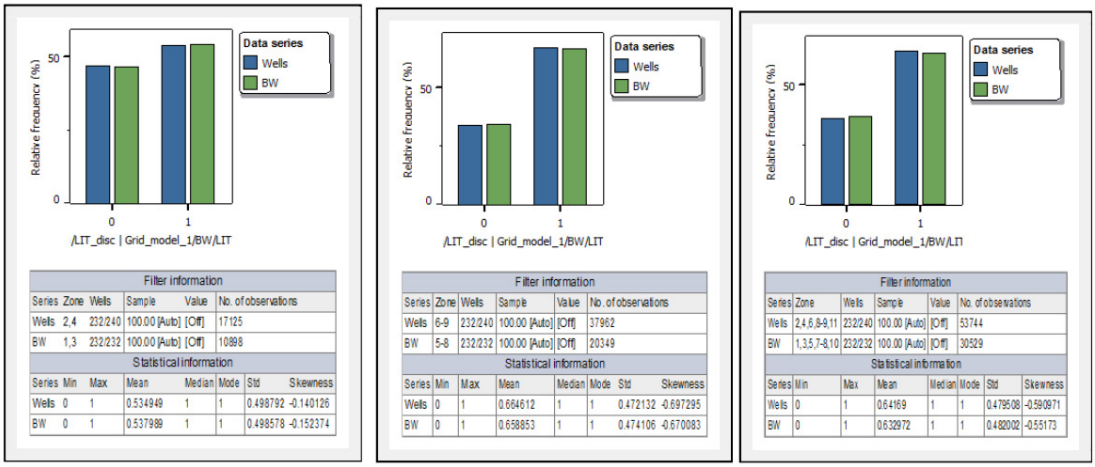

***Figure 2**. A comparison of the histograms of the distribution of values of the lithology parameter by well data (Wells RIGIS) and averaged over a 3D grid (BW). Layer J_1^1 + B_1 Layer J_1^{2a+b} + B_2 Formations J_1^1 , B_1 , B_2 , J_1^{2a} , J_1^{2b} , J_1^{2v}*

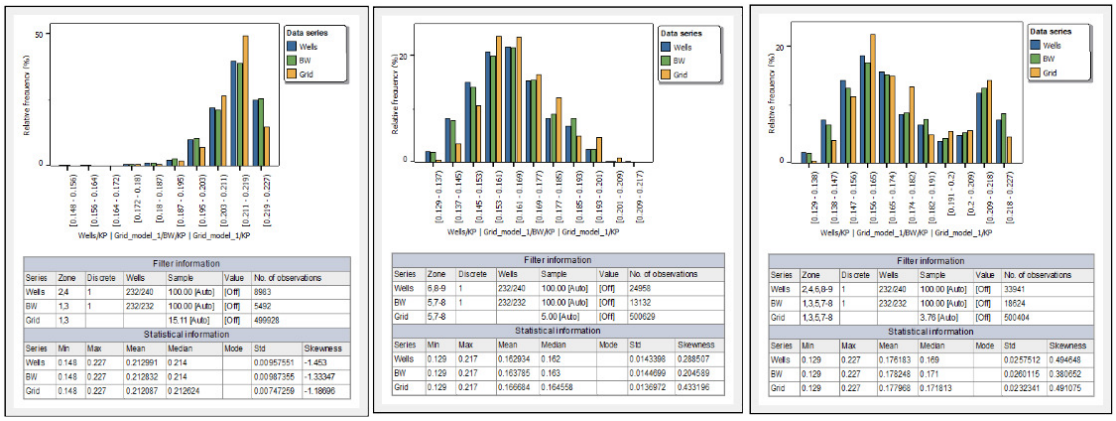

***Figure 3**.Histograms of the distribution of the porosity coefficient from well data (Wells RIGIS) averaged over a 3D grid (BW) and a porous cube (Grid). Layer J_1^1 + B_1 Layer J_1^{2a+b} + B_2 Formations J_1^1 , B_1 , B_2 , J_1^{2a} , J_1^{2b}*

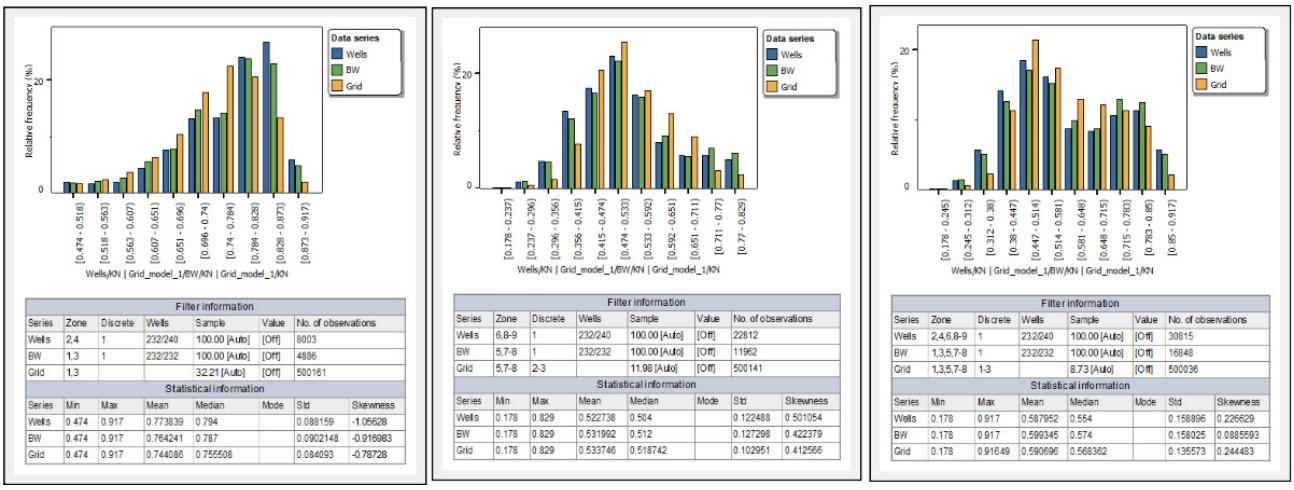

Figure 4. *The histograms of the distribution of the oil-gas saturation parameter from well data (Wells RIGIS) averaged over a 3D grid (BW) and a porous cube (Grid) Layer* $J_{1\text{-}1} + B_1$ *Layer* $J_{1\text{-}2}{}^{a+b} + B_2$ *Formations* $J_{1\text{-}1}$, B_1, B_2, $J_1{}^{2a}$, $J_1{}^{2b}$

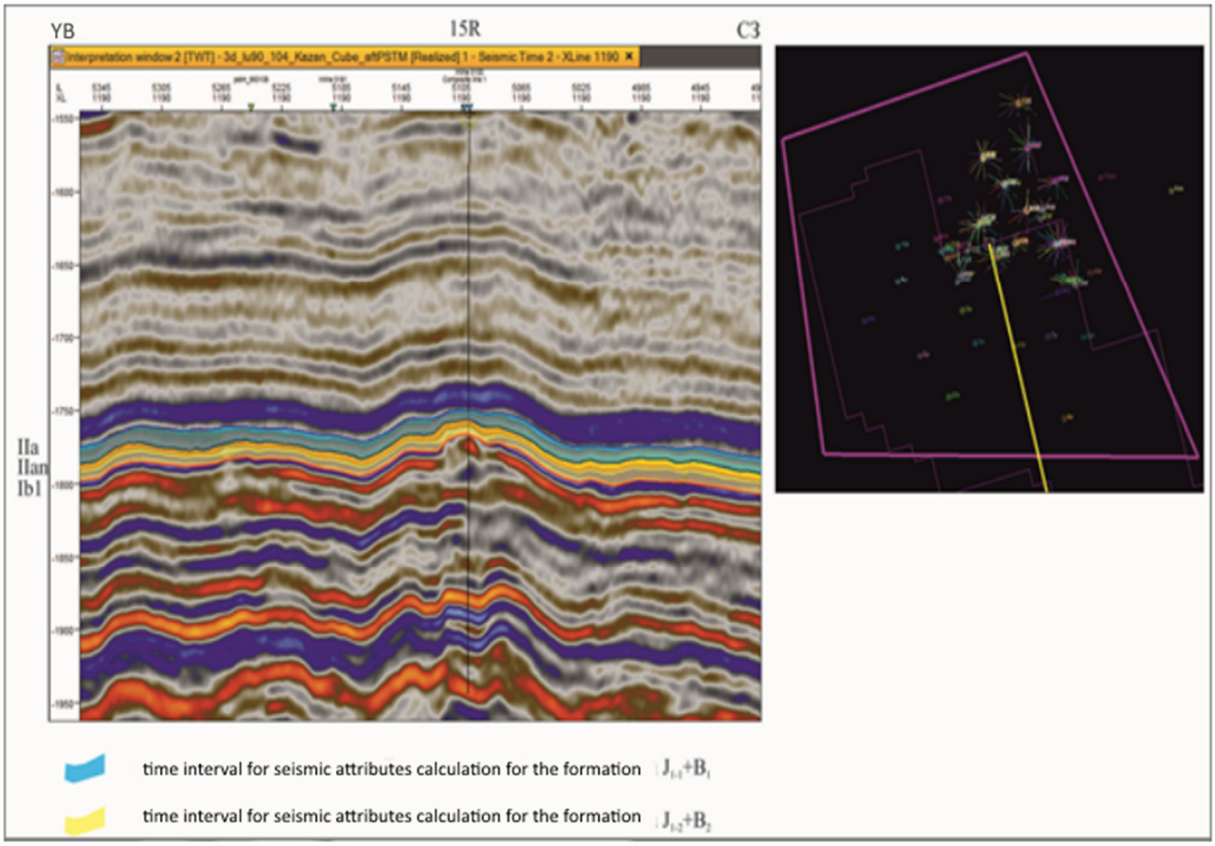

Figure 5. *Time windows for calculating seismic attributes for productive layers*

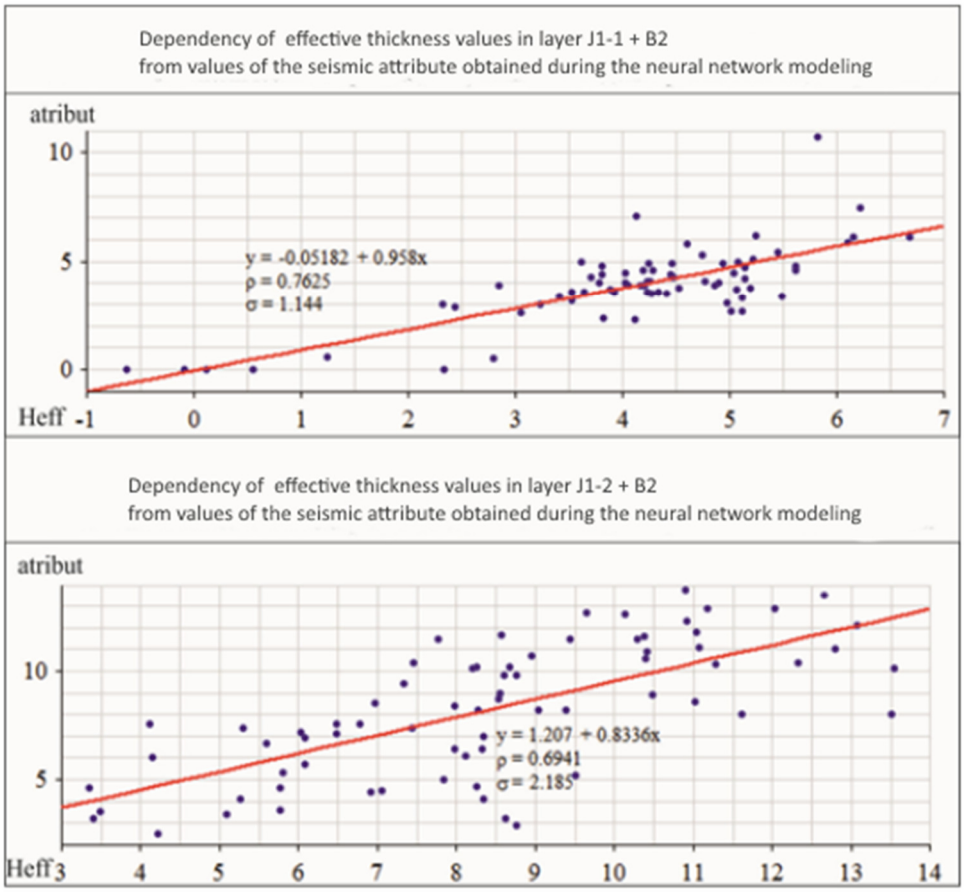

***Figure 6**. Dependences of values of effective thicknesses on productive strata from values of the seismic attribute obtained during the neural network modeling*

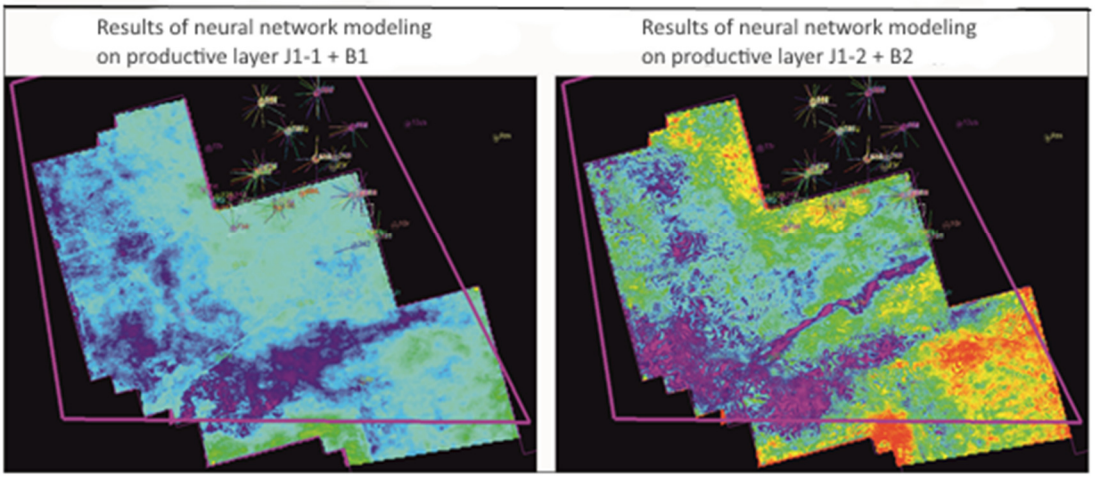

***Figure 7**. Maps of seismic attributes obtained in the course of neural network modeling*

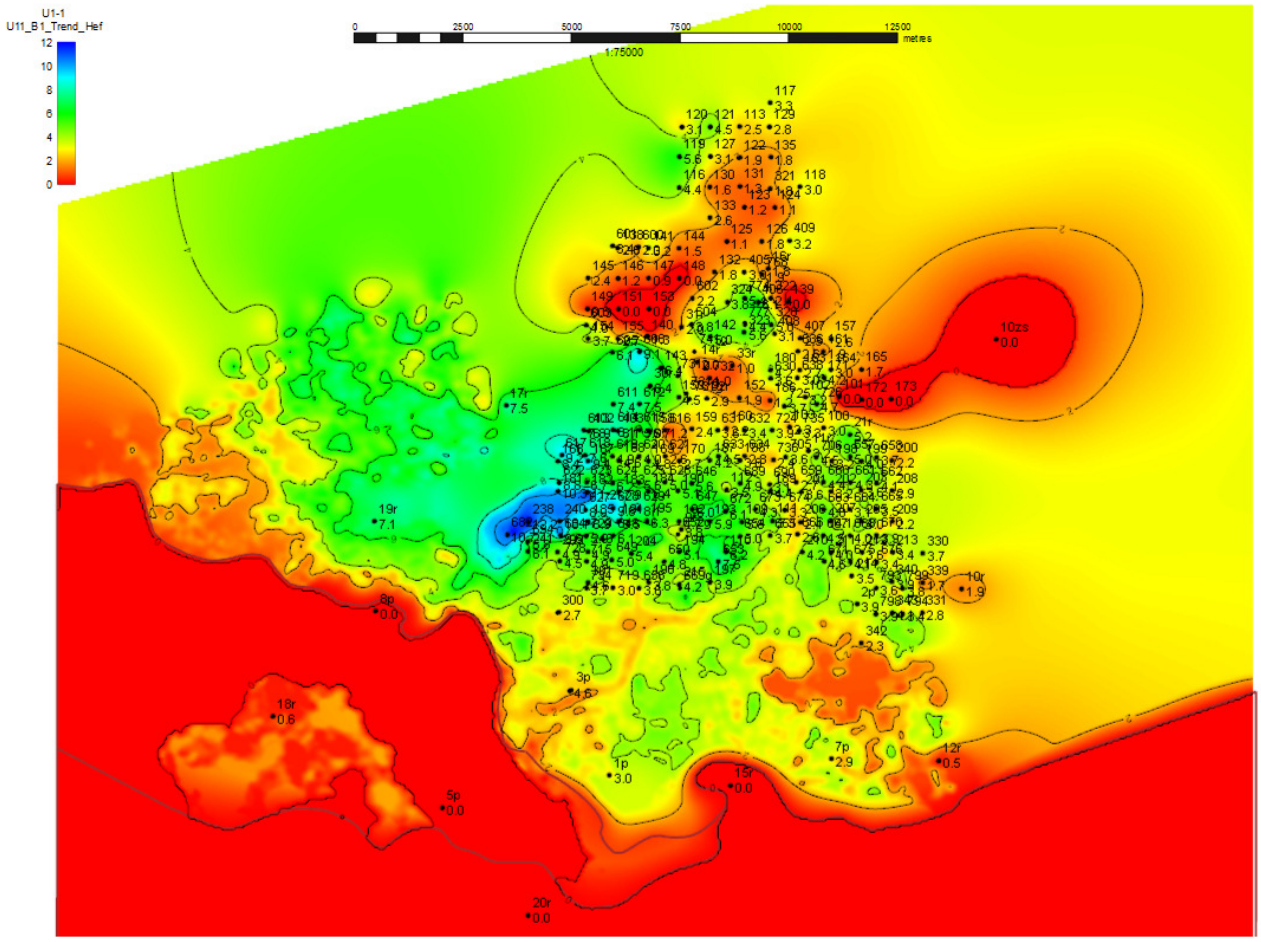

***Figure 8**. The prognostic map of the effective thicknesses of the productive layer J_1^1 + B_1 obtained in the course of neural network modeling*

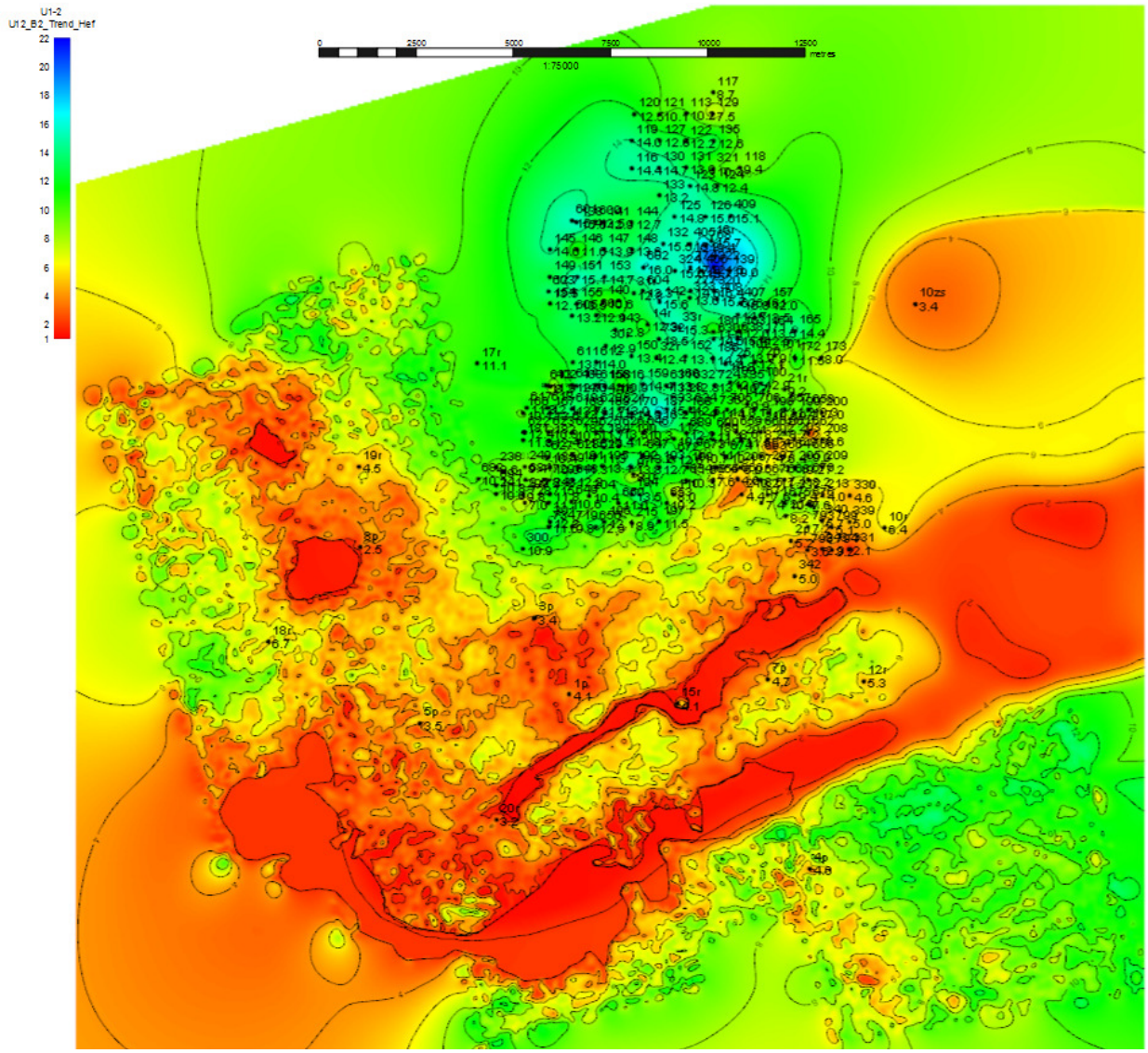

***Figure 9**. The prognostic map of the effective thicknesses of the productive layer J_1^2 + B_2 obtained in the course of neural network modeling*

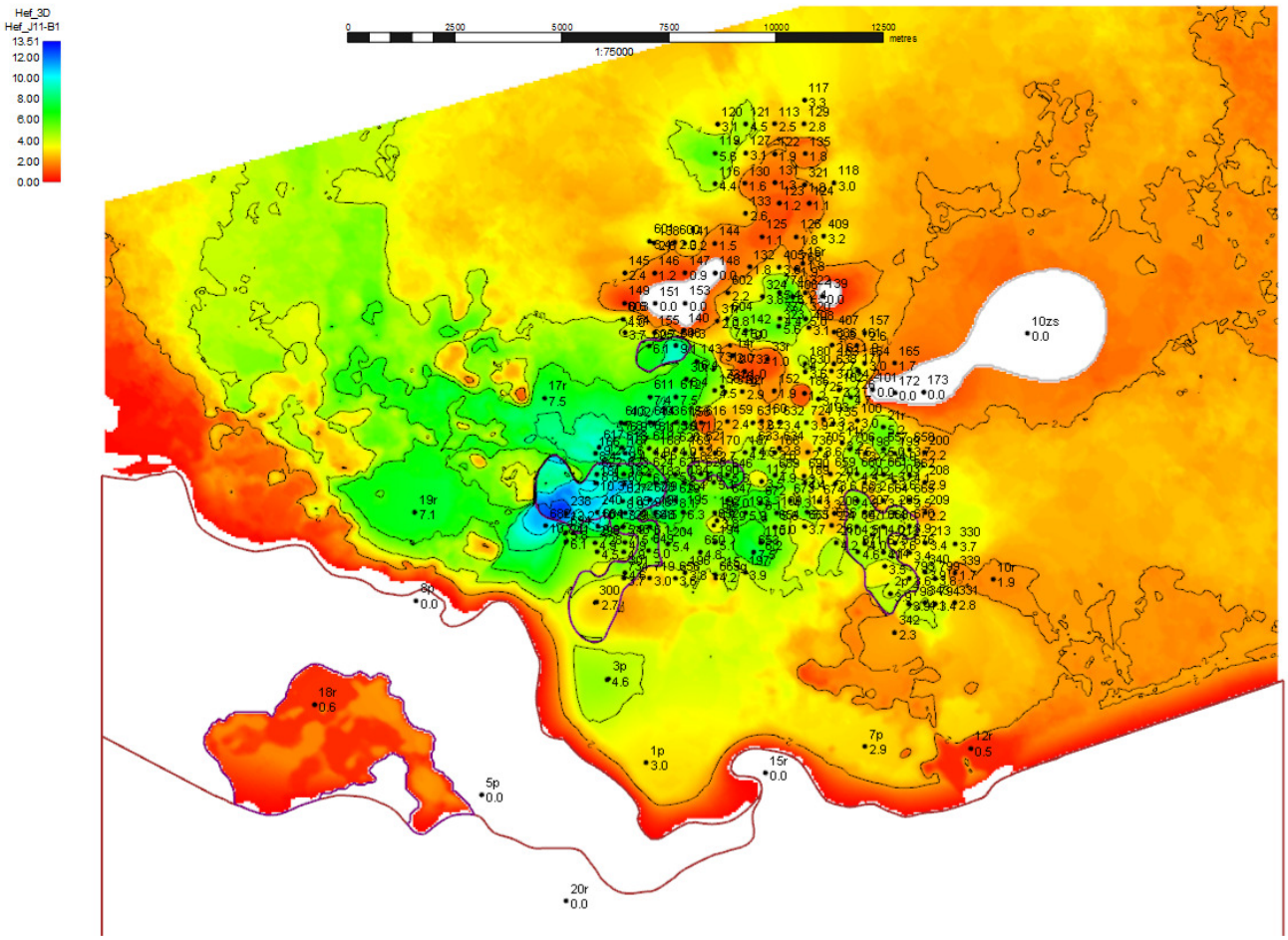

***Figure 10**. A map of the effective thicknesses of the productive layer $J_1^1 + B_1$, obtained from the lithology cube*

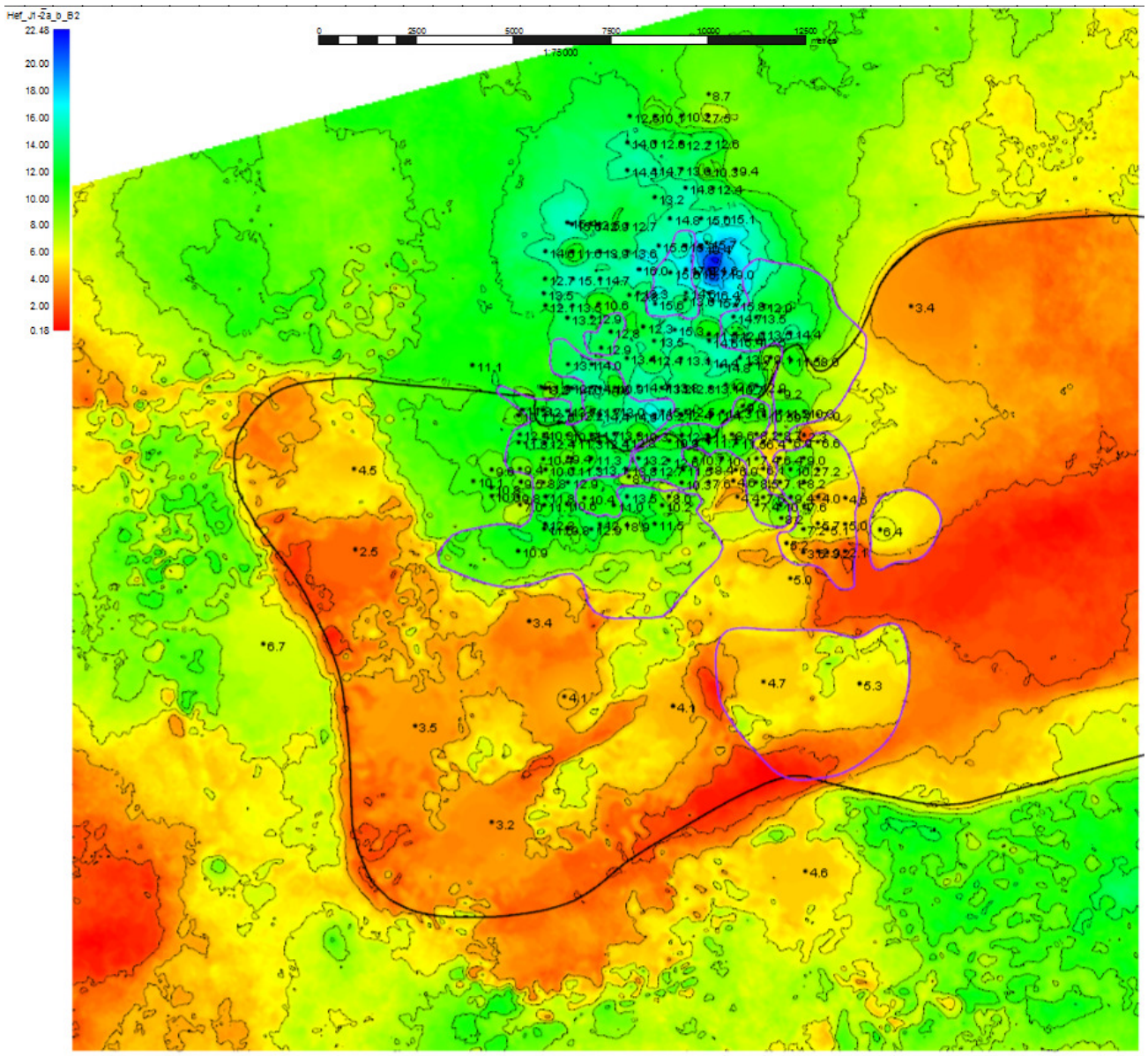

***Figure 11**. A map of the effective thicknesses of the productive layer J $_1$ ^{2} + B $_2$, obtained from the lithology cube*

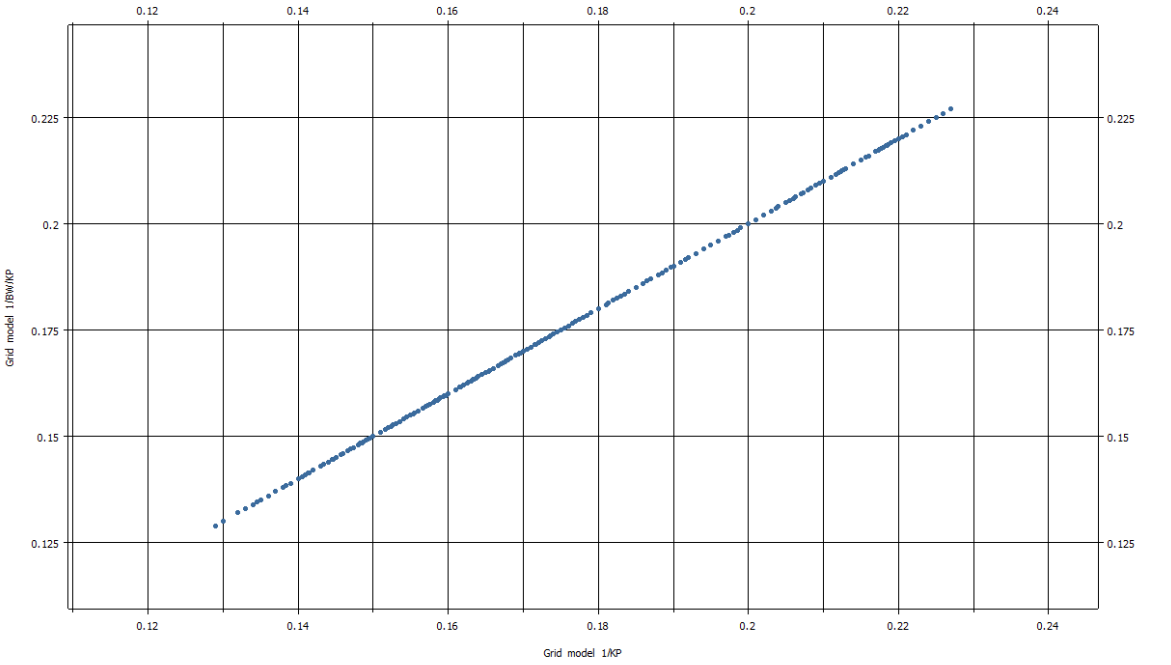

Filter information						
Series	Zone	Discrete	Wells	Sample	Value	No. of points
Series1	All		232/232	100.00 [Auto]	[Off]	18680
Statistical information						
Series	Correlation coefficient (Pearson)					
Series1	1					

***Figure 12**. Comparison of the values of BW cells and the resulting distribution of the porosity cube*

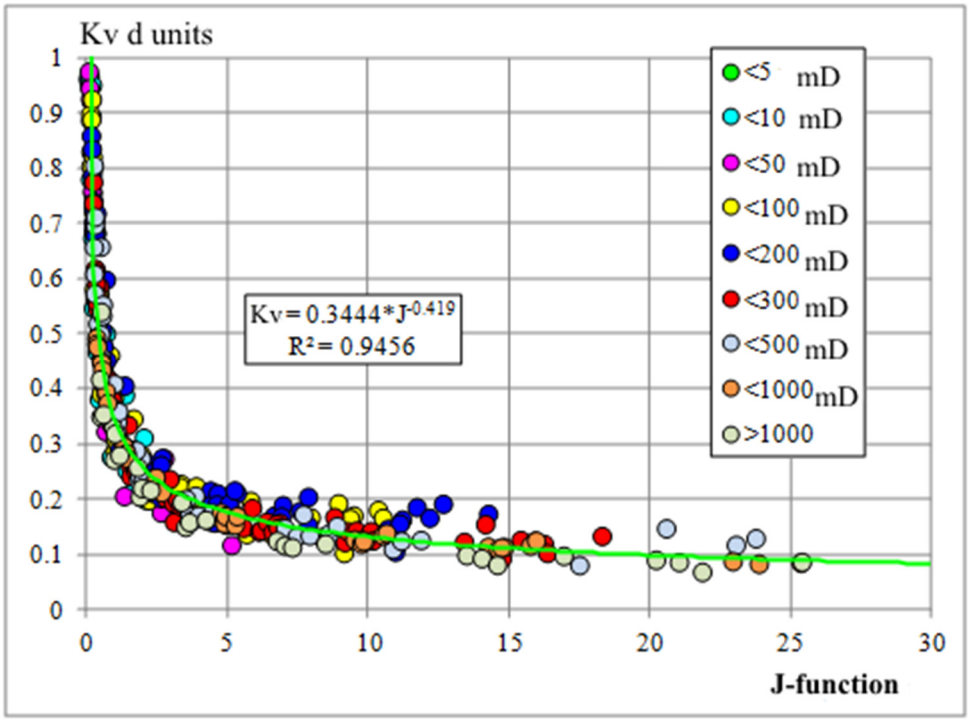

***Figure 13**. Dependence of the water saturation coefficient on the Buckley-Leverett J-function for the layer $J_1^1 + B_1$*

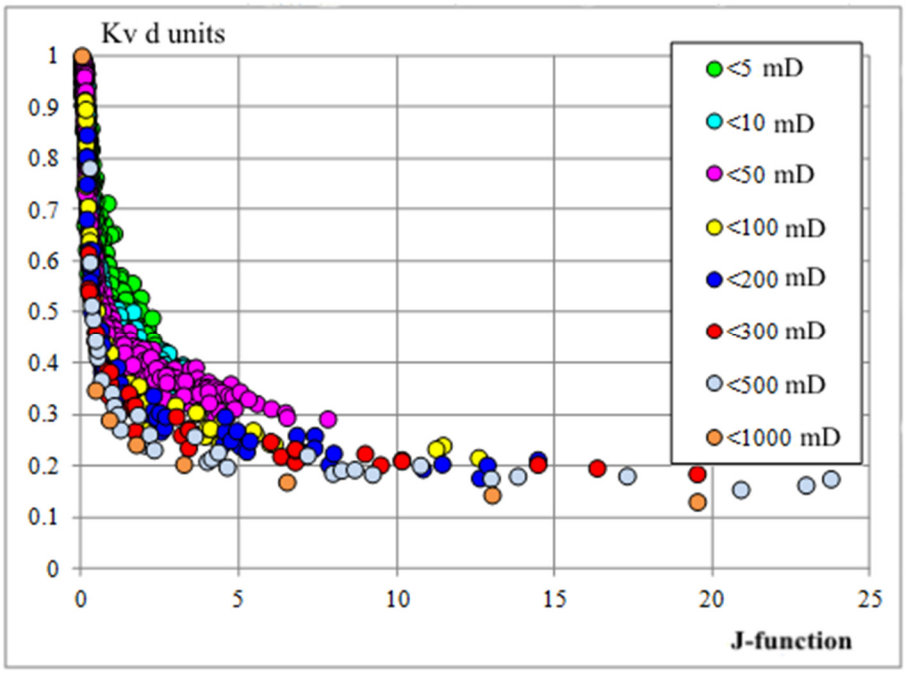

***Figure 14**. Comparison of the water saturation coefficient with the Buckley-Leverett J-function with a gradation by the permeability coefficient for the layer $J_{1}^{2} + B_{2}$*

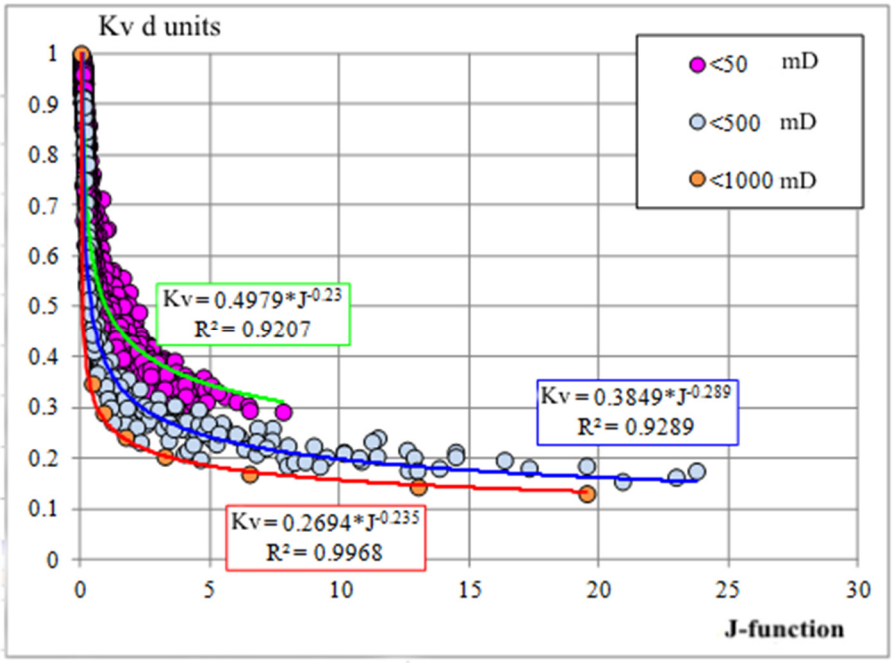

***Figure 15** .Dependences of the water saturation coefficient on the Buckley-Leverett J-function with a gradient on the permeability coefficient for the layer $J_{1\text{-}2} + B_{2}$*

$$J = \frac{3.183 \times Rs \times \sqrt{\frac{Kpr}{Kp}}}{\gamma \times \cos(\theta)}, \quad (1)$$

$$R_s^{(oil-water)} = R_s^{(air-water)} \cdot \frac{\cos\theta^{(oil-water)} \cdot \sigma^{(oil-water)}}{\cos\theta^{(air-water)} \cdot \sigma^{(air-water)}} = R_s^{(air-water)} * 0,375 \quad (2)$$

$R_s = (\delta_v - \delta_n) * 0,098 * h,$ (3)

$$h = \frac{R_k^{(\text{oil-water})}}{0,098 \cdot (\delta_v - \delta_n)}, \quad (4)$$

$$Kv = 0,3444 * \left(\frac{3,183 * 0,098 * \Delta h * \cdot (\delta_v - \delta_n) * \sqrt{\frac{K_{pr}}{K_p}}}{27}\right)^{-0,419}, \quad (5)$$

$$K_v = 2,8355 * (\Delta h * \sqrt{\frac{K_{pr}}{K_p}})^{-0,419} \quad (6)$$

$$Kv = 0,4979 * \left(\frac{3,183 * 0,098 * \Delta h * \cdot (\delta_v - \delta_n) * \sqrt{\frac{K_{pr}}{K_p}}}{27}\right)^{-0,23} \quad (7)$$

At $50 * 10^{-3}$ mkm $^2 \geq K_{pr} < 500 * 10^{-3}$ mkm ^{2} (8)

$$Kv = 0,3879 * \left(\frac{3,183 * 0,098 * \Delta N * \cdot (\delta_v - \delta_n) * \sqrt{\frac{K_{pr}}{K_p}}}{27}\right)^{-0,289} \quad (9)$$

At $K_{pr} \geq 500 * 10^{-3}$ mkm ^{2} (10)

$$Kv = 0,2694 * \left(\frac{3,183 * 0,098 * \Delta N * \cdot (\delta_в - \delta_н) * \sqrt{\frac{K_{pr}}{K_p}}}{27}\right)^{-0,235} \quad (11)$$

At $K_{pr} < 50 * 10^{-3}$ mkm ^{2} (12)

$$K_v = 1,6958 * (\Delta h * \sqrt{\frac{K_{pr}}{K_p}})^{-0,23} \quad (13)$$

At $50 * 10^{-3}$ mkm $^2 \geq K_{pr} < 500 * 10^{-3}$ mkm ^{2} (14)

$$Kv = 1{,}7965 * (\Delta h * \sqrt{\frac{K_{pr}}{K_p}})^{-0{,}289} \quad (15)$$

At $K_{pr} \geq 500 * 10^{-3}$ mkm ^{2} (16)

$$K_v = 0{,}9424 * (\Delta h * \sqrt{\frac{K_{pr}}{K_p}})^{-0{,}235} \quad (17)$$